



Aspects of Identifying a Damaged Site of a Wind Turbine Blade Using Power Spectral Density (PSD) Signature Curves and Energy Correlation Referenced Distance

Horacio V. Duarte¹

¹*Dept. de Engenharia Mecânica da Universidade Federal de Minas Gerais
Av Antônio Carlos 6627, CEP 31270-010, Belo Horizonte, Minas Gerais, Brasil*

Abstract. The following procedure is based on the energy correlation distance applied to the PSD (power spectral density) signature curves. Each PSD curve is calculated from the measurements at a point in the structure. The energy correlation distance between a single PSD curve and the set of all PSD curves of the measurement mesh is a metric. This metric is called the energy correlation referenced distance. In this work, to increase the difference between a healthy site and a damaged site, frequency bands of PSD curves are used. Using the temperature compensation properties of the referenced distance, the results are computed for a wide range of temperatures and then an analysis is made considering the structural constraints. The data used comes from a composite wind turbine blade whose data is housed in a public repository.

Keywords: Energy Correlation Referenced Distance, Temperature compensation, Structural restriction and Spatial damage position.

1 Introduction

There are many technical procedures for SHM, some of which come from the field of traditional modal analysis. There are many procedures to estimate the current state of health of a structure and its position, such as transmissibility functions (TF), that do not depend on excitation measurement[1, 2], curvature mode shapes[2, 3] and procedures using learning algorithms to identify modal parameter changes[1, 4].

In a great variety of methods, comparison between multivariate data is made using tests for specific statistic distribution[5]. The Root Mean Square Deviation (RMSD) method is a popular method comparing two sets, but not practical to multivariate data. In learning algorithm procedures, that usually deal with multivariate data, the Mahalanobis squared distance is the popular one. But this data must be multivariate multinormal distributed[4]. A recently proposed procedure is Energy Covariance and Correlation Distance introduced by Székely, Rizzo and Bakirov [6]. The short definition of Energy Distance is a distance between distributions[7]. It applies to random vectors in arbitrary dimensions, and the methodology requires only the assumption of finite first moments[7]. Beyond its simplicity, the main interest in Energy Correlation Distance, is that Energy distance does not require specific statistical distribution[7, 8].

The Energy Correlation Referenced Distance method relies only on experimental measurements to detect damage. This work will employ power spectral densities, PSDs, the PSD is a signature of the structure under linear dynamic excitation. If there are no temperature changes, energy distances between the PSD curves computed from measurements at one point at different times should be equal. There are many empirical relations to correct the measurement to reference temperature. The common idea behind all those procedures is that if the variables of interest change only with temperature, then all variables dependent on temperature change by the same amount.

2 Methodology

The Coefficient of Covariance and Correlation Distances concepts have been presented without the technical details available in the original work by Székely et al.[6]. Practical discussion and examples of

use of this statistics can be found in Duarte[9].

As stated in Szekely[10], the $\mathcal{R}_n(X, Y)$ coefficient lies in the $-1 \leq \mathcal{R}_n(X, Y) \leq 1$ interval, but $0 \leq |\mathcal{R}_n(X, Y)| \leq 1$ satisfies the triangle inequality and the metric axiom[10]. Distance correlation can be applied as an index of dependence [6], and there is no restriction related to distribution type[8].

Referenced distance is a metric distance between a sensor's response in a frequency range and all sensor responses in the same frequency band. This metric distance is independent of temperature as its reference is the whole set at same temperature (the variables that change by the same amount); in other words, this referenced distance should be constant for all temperatures, Duarte[9].

This referenced distance is implemented by dividing the PSD curve into frequency intervals ($s = a, b, \dots, f$). Comparisons are made for each frequency band at measurement sensor i and temperature T , $X_s^i(T)$. The $\Omega_s(T)$ reference is the set of all grid measurement points taken at frequency band s , $\Omega_s(T) = \cup_i X_s^i(T)$, at temperature T . As $X_s^i(T) \in \Omega_s(T)$, $X_s^i(T) = \Omega_s[i](T)$, then, at each measurement position i there is the metric referenced distance

$$\mathcal{D}_i^s(T) = \mathcal{R}_n(X_s^i(T), \Omega_s(T)) = \mathcal{R}_n(\Omega_s[i], \Omega_s)_T \quad (1)$$

computed using the energy distance \mathcal{R}_n between structural response at position i , $X_s^i(T)$, and the complete response set $\Omega_s(T)$ at frequency band s .

The expectation is that the $\mathcal{D}_i^s(T)$ between a single point $\Omega_s[i]$ to this reference, Ω_s , will change less for sets taken at different temperatures. As there are healthy and damaged sets and comparison between them, some improvements should be made on notation. In Table 1 the nomenclature, definitions and simplified notation for different distances.

Table 1. Referenced distance \mathcal{D}_i^s at sensor position i for frequency band s and temperature T

Referenced Distance	Nomenclature	Definition	Simplified Notation
General Case	$\mathcal{D}_i^s(T)$	$\mathcal{R}_n(\Omega_s[i], \Omega_s)_T$	-
For Health set H	$\mathcal{D}_{h,H}^s[i](T)$	$\mathcal{R}_n(\Omega_s^H[i], \Omega_s^H)_T$	$h[i] \times H$
For Damaged set D	$\mathcal{D}_{d,D}^s[i](T)$	$\mathcal{R}_n(\Omega_s^D[i], \Omega_s^D)_T$	$d[i] \times D$
From Damaged point, i , to set H	$\mathcal{D}_{d,H}^s[i](T)$	$\mathcal{R}_n(\Omega_s^D[i], \Omega_s^H)_T$	$d[i] \times H$
From health point, i , to set D	$\mathcal{D}_{h,D}^s[i](T)$	$\mathcal{R}_n(\Omega_s^H[i], \Omega_s^D)_T$	$h[i] \times D$

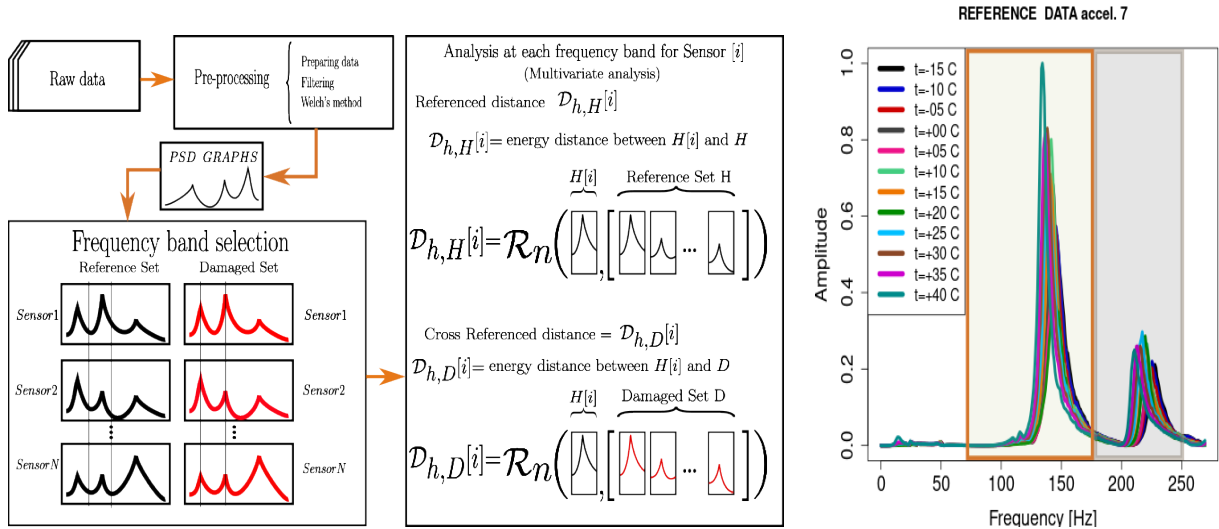


Figure 1. On the left side the flowchart for the damage detection method using referenced distance based on energy correlation distance for temperature changing environment. On the right side the PSD curve for the 7th sensor showing the two frequency band used in this work, 70 to 180 Hz and 180 to 250 Hz. Extracted from Duarte[9]

PDS frequency bands, including a natural frequency, have been used to improve the referenced distance's precision. The whole procedure is presented in the Figure 1 flowchart, where, $\mathcal{D}_{h,H}[i]$, the referenced distance is defined for the i sensor, and for the same sensor $\mathcal{D}_{h,D}[i]$ is the cross-referenced

distance. The referenced distance, $\mathcal{D}_{h,H}[i]$, should be constant. Damage can be identified if a new measurement set, D , at same temperature or temperature range, results in $\mathcal{D}_{h,H}[i] \neq \mathcal{D}_{h,D}[i]$.

In Fig. 1 one aspect that stands out is the definition of referenced distance comparing a vector and a vector set (Root Mean Square Deviation, RMSD, that works comparing pair of vectors can not be used). On the right side of Fig. 1 there are twelve PSD curves one for each temperature in the range between -15 to 40 Celsius for the sensor 7th. In this graph, the two frequency bands that will be analyzed using the referenced distance technique are highlighted. This data is obtained from a public benchmark to test the procedure; the database comes from a wind turbine blade housed in the Zenodo repository[11].

3 Measurement Data and Analysis

This section presents the experimental results using the energy distance correlation coefficient \mathcal{R}_n and referenced distance \mathcal{D}_i^s . Data come from a wind turbine blade of a public benchmark stored in the Zenodo repository[11]. This wind blade is supported only at a hub in a fix-free set-up during dynamic testing. An electromechanical shaker was utilized for the dynamic excitation[12]. This system was mounted in a climate chamber where temperature and humidity are kept constant.

In this dataset there are two types of sensors, accelerometers and strain gauges. There are two configurations for the strain gauges, but the positions of the accelerometers do not change in both configurations and can be seen as a red dot in Fig. 2. In this figure the blade structure was extracted from Tatsis K. et al[2] and sensor position from Ou Y et al[12]. The following results are only for accelerometers.

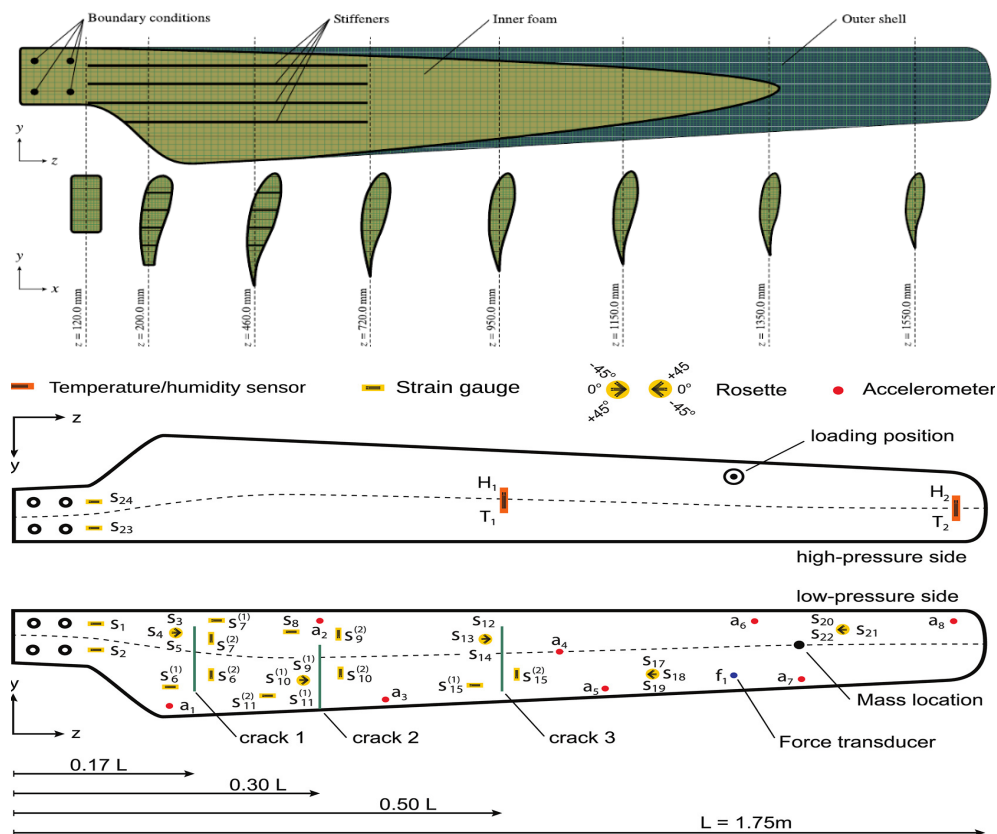


Figure 2. Wind turbine blade structure, extracted from Tatsis K. et al[2], sensor configuration and damage position, extracted from Ou Y. et al[12]. The accelerometer position is shown as a red dot point.

Data are from different structural scenarios, Table 2, a healthy or reference set is labeled R case, the others sets D , E and F are from a different damaged levels, Table 2. For each crack the length is 5×10^{-2} m, 4×10^{-3} m depth and 1.5×10^{-3} m width getting through the 0.93×10^{-3} m thick coating shell[12][2]. The difference between the cases are the crack position and its number, Fig. 2.

At each temperature 20 experiments are done for R case and 5 results are available for each of the damaged cases D , E and F . These tests were conducted using white noise input and all data are in time

Table 2. Structural scenarios

Case	Structural Status			Experiments
R	Health			20
D	Crack 1, $l_1 = 5 \times 10^{-2}$ m			5
E	Crack 1, $l_1 = 5 \times 10^{-2}$ m	Crack 2, $l_2 = 5 \times 10^{-2}$ m		5
F	Crack 1, $l_1 = 5 \times 10^{-2}$ m	Crack 2, $l_2 = 5 \times 10^{-2}$ m	Crack 3, $l_3 = 5 \times 10^{-2}$ m	5

domain, obtained at 1666 Hz sampling rate. To obtain one PSD curve the results for 5 experiments are employed, so there is a single PSD curve for the D , E , F cases and 4 PSD curves for the healthy or reference set, the R case

4 Results and Analyzes

Some results for referenced distances comparing the structures in different damage levels for the temperature range are presented in Fig. 3, Fig. 4, Fig.5, Fig.6. Figure 3 show graphics for accelerometer 1 at second and third frequency band for $R \times E$ cases. The referenced distances $\mathcal{D}_{h,H}^s[i]$, plotted in green lines and the damaged referenced distance $\mathcal{D}_{d,D}^s[i]$ in red lines. For the third frequency band, third graph from left in Fig. 3, although those lines are not perfectly parallel to the temperature axis, no temperature dependence can be observed. For the first panel on the left of Fig. 3, for distances $\mathcal{D}_{h,H}^s$, green line and

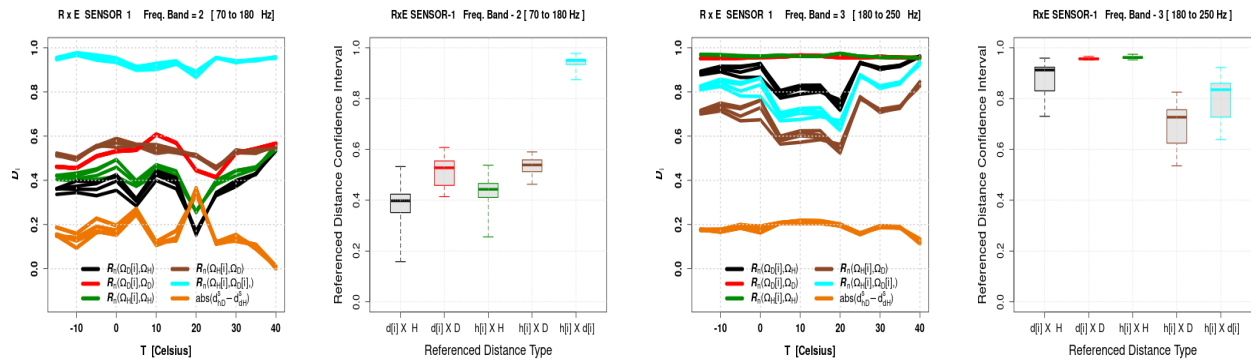


Figure 3. Sensor 1, referenced distances \mathcal{D}_i^s for $R \times E$ cases. From the left side, the first graph shows the results for $\mathcal{D}_i \times T$, the second shows its confidence interval for the entire temperature range, both from the second frequency band s . The third graph, $\mathcal{D}_i \times T$, is also for sensor 1 using the third frequency band s , in sequence the graph with its confidence interval.

$\mathcal{D}_{d,D}^s$, red line, there are a random behavior and there is no dependence on temperature also. Therefore, the main hypothesis that the referenced distances $\mathcal{D}_{h,H}^s$ and the damaged referenced distance $\mathcal{D}_{d,D}^s$ can compensate for the temperature variation is correct and has been empirically proven.

This is a behavior that is repeated in all the cases analyzed, the following graphs Fig. 4, Fig.5, Fig.6 for different damage situations, are a sample that illustrates this. In the first panel of the Fig. 4 the healthy referenced distance $\mathcal{D}_{h,H}^s$, green line, and the damaged referenced distance $\mathcal{D}_{d,D}^s$, red line, are parallel to the temperature axis but overlap each other without a gap between them to discern damaged and healthy state. Similar situation can be observed in the first panel of the Fig. 5 and in the third panel of the Fig. 6, also in the last graph of Fig. 3.

The last graph in the Fig. 3, shows the data dispersion between the maximum and minimum limits for referenced distances $\mathcal{D}_{h,H}^s$ - green line, $\mathcal{D}_{d,D}^s$ - red line, $\mathcal{D}_{d,H}^s$ - in black lines and $\mathcal{D}_{h,D}^s$ - brown lines that is plotted in the third graph Fig. 3. The data dispersion of cross referenced distance $\mathcal{D}_{d,H}^s$, black lines, show overlapping intervals for $\mathcal{D}_{h,H}^s$ - green line, and $\mathcal{D}_{d,D}^s$ - red line. But $\mathcal{D}_{h,D}^s$, brown line, is not within the dispersion distances $\mathcal{D}_{h,H}^s$ and $\mathcal{D}_{d,D}^s$ and this is a clear indication of damage.

5 Using Cross referenced distances $\mathcal{D}_{d,H}^s$, $\mathcal{D}_{h,D}^s$ to determine damage position

The cross referenced distances $\mathcal{D}_{d,H}^s$ and $\mathcal{D}_{h,D}^s$ were used to determine a positive damage when the reference distance $\mathcal{D}_{h,H}^s$ and $\mathcal{D}_{d,D}^s$ are too close. The third graph on Fig. 3, the first on Fig. 4 and Fig.

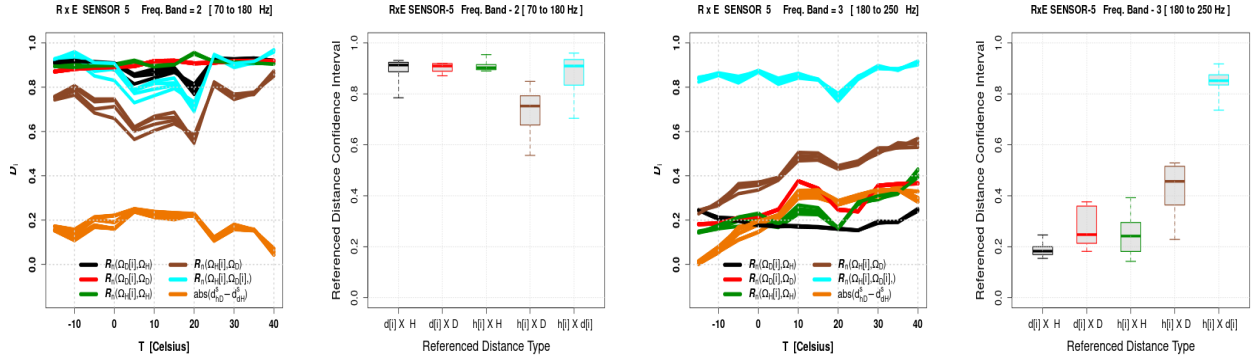


Figure 4. Sensor 5, referenced distances \mathcal{D}_i^s for $R \times E$ cases. The $\mathcal{D}_i \times T$, and its confidence interval for second and third frequency band s.

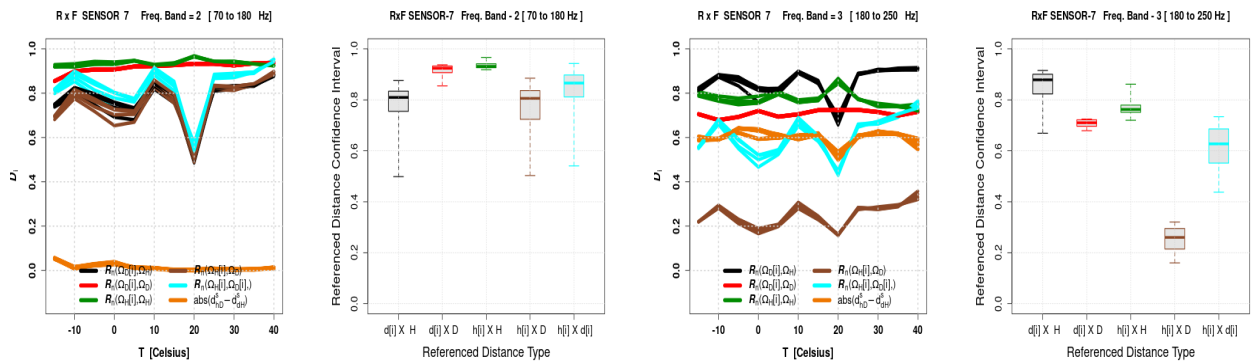


Figure 5. Sensor 7, referenced distances \mathcal{D}_i^s for $R \times F$ cases. The $\mathcal{D}_i \times T$, and its confidence interval for second and third frequency band s.

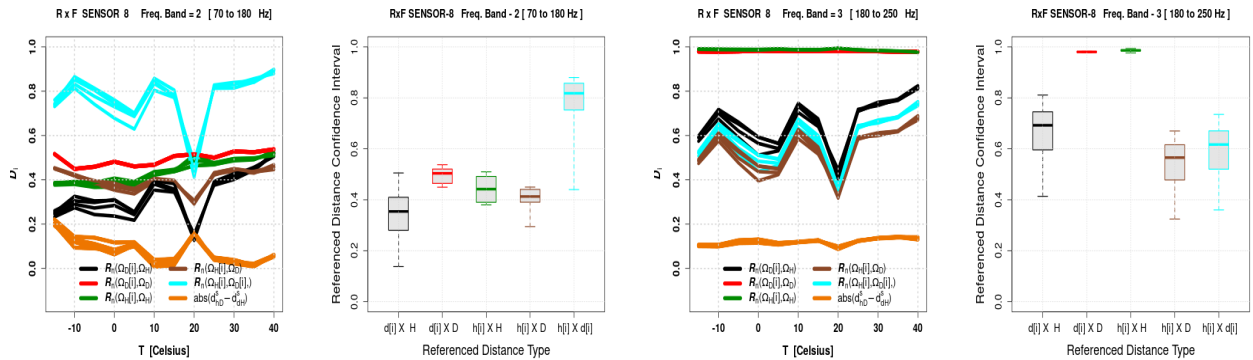


Figure 6. Sensor 8, referenced distances \mathcal{D}_i^s for $R \times F$ cases. The $\mathcal{D}_i \times T$, and its confidence interval for second and third frequency band s.

5 and the third graph on Fig. 6 show another interesting feature. In these graphics, the cross referenced distances $\mathcal{D}_{d,H}^s$, black lines, and $\mathcal{D}_{h,D}^s$ brown lines, seemed to maintain the same distance regardless of the shape of the curve. Highlighting these characteristics, the absolute value of $|\mathcal{D}_{h,D}^s - \mathcal{D}_{d,H}^s|$ was plotted using an orange line in these figures. Another aspect that should be emphasized is that the absolute value of this difference seems to depend on the position and level of damage.

In the Fig. 7, except for the last 2 sensors, $|\mathcal{D}_{h,D}^s - \mathcal{D}_{d,H}^s|$ is almost constant for all sensors and presents small increase with damage level. One hypothesis to explain this is that there may be significant damage near the hub. In the Fig. 7, the graphs for $\mathcal{D}_{h,D}^s - \mathcal{D}_{d,H}^s$ signal that odd and even sensors, located on opposite sides, have displacement in opposite directions that resembles a torsion mode. This twisting motion changes direction between sensors 4 and 5.

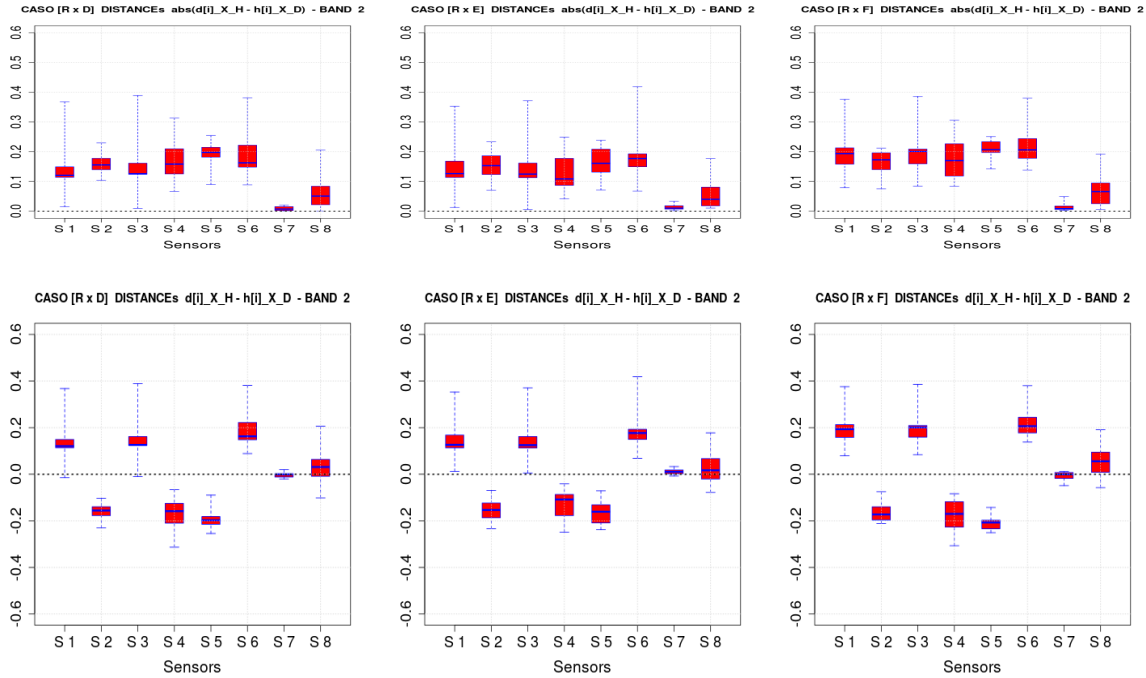


Figure 7. In the upper row $|\mathcal{D}_{h,D}^s - \mathcal{D}_{d,H}^s|$ below $\mathcal{D}_{h,D}^s - \mathcal{D}_{d,H}^s$ for the $R \times D$ case, on the left column, at center $R \times E$ case, on the right side $R \times F$. Second frequency band.

The third aspect is the almost zero value for $\mathcal{D}_{h,D}^s - \mathcal{D}_{d,H}^s$ at sensor 7 for all damage levels. The difference $\mathcal{D}_{h,D}^s - \mathcal{D}_{d,H}^s = 0$ means that there is no difference between the displacements in that position for the damaged and undamaged case. The same behavior, $\mathcal{D}_{h,D}^s - \mathcal{D}_{d,H}^s = 0$, can also be seen in Fig. 8 at sensor 6 for the third frequency band.

An inspection in Fig. 2 indicates that both sensors are very close to the shaker's drive point. The proximity to the drive point explains the almost similar displacement for the damaged and health structure. There is movement, but it is limited by the course of the shaker and this is most significant at a natural frequency when displacements tend to be greater.

The results in the first row of the of graphs in Fig. 8 show that sensor 2 and sensor 7 stand out and that the $|\mathcal{D}_{h,D}^s - \mathcal{D}_{d,H}^s|$ values increase for all sensors with increasing damage level.

The statistic $\mathcal{D}_{h,D}^s - \mathcal{D}_{d,H}^s$, in the second row, signal an increasing difference between sensors 1, 2 and 3 as they grow in opposite directions, with sensor 2 having the greatest influence. Due to its position in a region of high stiffness in the structure, sensor 2 stands out already at the lowest level of damage and is always prominent as the level of damage increases, suggesting that the place or places where faults occur are nearby it.

Using only this information, the regions near sensors 1, 2, 3 and 7 should receive a detailed inspection. However, there are some doubts about the role of the force transducer in the response of sensor 7 for the third frequency band.

6 Final Remarks

The damage region has been successfully located and the shaker position has been also successfully located. Shaker's position was not a desired result. It showed that it had an influence on the results. The alert level needs to be statistically quantified in further work.

References

- [1] S. Chesné and A. Deraemaeker. Damage localization using transmissibility functions: a critical review. *Mechanical Systems and Signal Processing*, 2013.

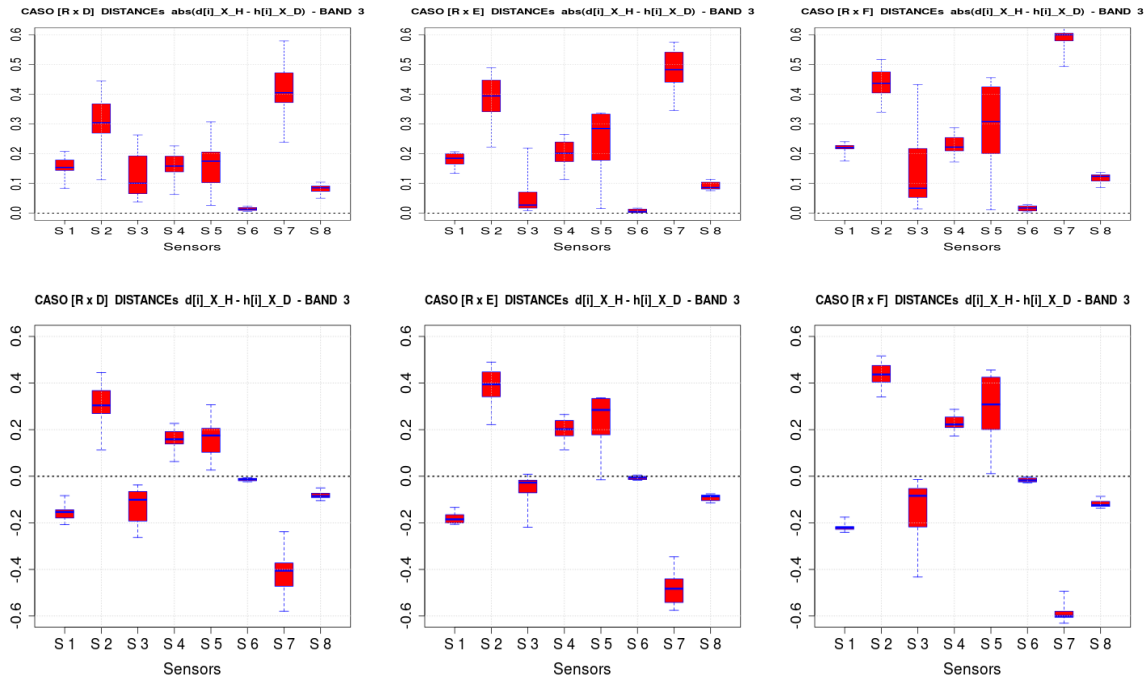


Figure 8. In the upper row $|\mathcal{D}_{h,D}^s - \mathcal{D}_{d,H}^s|$ below $\mathcal{D}_{h,D}^s - \mathcal{D}_{d,H}^s$ for the $R \times D$ case, on the left column, at center $R \times E$ case, on the right side $R \times F$. Third frequency band.

- [2] K. Tatsis, Y. Ou, V. K. Dertimanis, M. D. Spiridonakos, and E. N. Chatzi. Vibration-based monitoring of a small-scale wind turbine blade under varying climate and operational conditions. Part II: A numerical benchmark. *Structural Control and Health Monitoring*, vol. 28, n. 6, 2021.
- [3] W. Fan and P. Qiao. Vibration-based damage identification methods: A review and comparative study. *Structural Health Monitoring*, vol. 10(1), pp. 83–111, 2011.
- [4] T. Nguyen, T. H. Chan, and D. P. Thambiratnam. Field validation of controlled monte carlo data generation for statistical damage identification employing mahalanobis squared distance. *Structural Health Monitoring*, vol. 13(4), pp. 473–488, 2014.
- [5] D. S. Rabelo, V. S. Jr, R. M. F. Neto, and H. B. Lacerda. Impedance-based structural health monitoring and statistical method for threshold-level determination applied to 2024-t3 aluminum panels under varying temperature. *Structural Health Monitoring*, vol. 16(4), pp. 365–381, 2017.
- [6] G. J. Székely, M. L. Rizzo, and N. K. Bakirov. Measuring and testing independence by correlation of distances. *The Annals of Statistics*, vol. 35, n. 6, pp. 2769–2794, 2007.
- [7] M. L. Rizzo and G. J. Székely. Energy distance. *WIREs Computational Statistics*, vol. 8, pp. 27–38, 2016.
- [8] G. J. Székely and M. L. Rizzo. Brownian distance covariance. *The Annals of Applied Statistics*, vol. 3, n. 4, pp. 1236–1265, 2009.
- [9] H. V. Duarte and L. V. Donadon. Frequency-based damage detection method using energy correlation distance in temperature changing environment. *Structural Health Monitoring*, in press.
- [10] G. J. Székely and M. L. Rizzo. The distance correlation t-test of independence in high dimension. *Journal of Multivariate Analysis*, vol. 117, pp. 193–213, 2013.
- [11] Y. Ou, K. Tatsis, V. Dertimanis, M. Spiridonakos, and E. Chatzi. Vibration-based Monitoring of a Small-scale Wind Turbine Blade Under Varying Climate Conditions. Part I: An Experimental Benchmark, 2019.
- [12] Y. Ou, K. Tatsis, V. K. Dertimanis, M. D. Spiridonakos, and E. N. Chatzi. Vibration-based monitoring of a small-scale wind turbine blade under varying climate and operational conditions. Part I: An experimental benchmark. *Structural Control and Health Monitoring*, vol. 28, n. 6, 2020.